Title
Baculovirus Actin-Based Motility Drives Nuclear Envelope Disruption and Nuclear Egress

Journal
Current Biology, 28(13)

ISSN
0960-9822

Authors
Ohkawa, Taro
Welch, Matthew D

Publication Date
2018-07-01

DOI
10.1016/j.cub.2018.05.027

Peer reviewed

Published in final edited form as:

Curr Biol. 2018 July 09; 28(13): 2153–2159.e4. doi:10.1016/j.cub.2018.05.027.

Baculovirus actin-based motility drives nuclear envelope disruption and nuclear egress

Taro Ohkawa[1] and **Matthew D. Welch**[1,*]

[1]Department of Molecular & Cell Biology, University of California, Berkeley CA 94720, USA

Summary

Viruses that replicate in the host cell nucleus face challenges in usurping cellular pathways to enable passage through the nuclear envelope [1]. Baculoviruses are enveloped, double-stranded DNA viruses that infect lepidopteran insects and are tools for protein expression, cell transduction and pest management [2, 3, 4]. The type species *Autographa californica* M nucleopolyhedrovirus (AcMNPV) shares with other pathogens an ability to assemble host actin monomers (G-actin) into actin filaments (F-actin) to drive motility [5]. During early infection, actin-based motility in the cytoplasm speeds AcMNPV transit to the nucleus and passage through nuclear pores, enabling nuclear ingress [6, 7]. During late infection, AcMNPV assembles F-actin within the nucleus [8], which is essential for virus production [9, 10]. However, the function of nuclear F-actin is poorly understood [11], and its mechanistic role in AcMNPV infection was unknown. We show that AcMNPV mobilizes actin within the nucleus to promote egress. AcMNPV nucleocapsids exhibit intranuclear actin-based motility, mediated by the viral protein P78/83 and the host Arp2/3 complex. Viral motility drives transit to the nuclear periphery and is required for viruses to enter protrusions of the nuclear envelope. Moreover, actin polymerization is necessary for viral disruption of nuclear envelope integrity during egress. In the cytoplasm, viruses use actin-based motility to reach the plasma membrane to enable budding. Our results demonstrate that pathogens can harness actin polymerization to disrupt the nuclear envelope. Employing actin for nuclear envelope disruption may reflect viral appropriation of normal functions of nuclear actin in nuclear envelope integrity, stability, and remodeling.

Keywords

baculovirus; AcMNPV; actin-based motility; viral egress; nuclear actin; Arp2/3 complex

[*]Corresponding author and lead contact: MCB Department, 301 Life Sciences Addition, Berkeley, CA 94720-3200, (510) 643-9019, welch@berkeley.edu.

Declaration of Interests

The authors declare no competing interests.

Author Contributions:

Conceptualization, T. O. and M. D. W. Methodology, T. O. and M. D. W. Investigation, T. O. Writing, T. O. and M. D. W. Funding Acquisition, M. D. W. Supervision, M. D. W.

Results and Discussion

To define the essential role of nuclear actin in baculovirus progeny production, we visualized the association of individual viral nucleocapsids with F-actin during budded virus (BV) production using a recombinant virus that expresses the major viral capsid protein VP39 fused to three copies of the fluorescent protein Dronpa (AcMNPV-3Dr; this virus grew with normal kinetics but to a 3-fold lower titer than wild type, Figure S1A). We then carried out live cell imaging in cultured *Trichoplusia ni* High Five cells expressing the F-actin marker Lifeact fused with mCherry (Lifeact-mCherry). We observed that newly assembled nucleocapsids underwent actin-based motility within the nucleus, generating characteristic actin comet tails (Figure 1A and B; Video S1, segment 1). The first instance of nuclear actin-based motility could be visualized at 12 ± 2 (mean ± SD) hours post-infection (hpi) (Figure 1A). This was followed by a pronounced burst of more frequent motility beginning at 16 ± 3 hpi, during which many moving viruses appeared within a relatively short time interval (~75 min). The timing of motility initiation corresponded with the formation of viral replication centers or virogenic stroma, which were observed by expression of VP39 fused with mCherry (VP39-mCherry) as dim structures starting at 13 ± 2 hpi, and then bright structures starting at 16 ± 3 hpi. Thus, AcMNPV undergoes intranuclear actin-based motility, and this occurs concomitantly with viral progeny production.

To examine the mechanism of intranuclear nucleocapsid motility and compare it with motility in the cytoplasm during viral ingress, we measured key motility parameters. The speed of intranuclear motility was 13 ± 3 μm/min (mean ± SD) (Figure 1C), similar to what we previously observed for cytoplasmic motility (14 ± 4 μm/min) [6]. We additionally assessed the involvement of the viral P78/83 protein, an essential minor capsid protein that is conserved in lepidopteran NPVs and acts as a nucleation-promoting factor that activates the host Arp2/3 complex to assemble branched F-actin from G-actin [8]. We used the AcMNPV-3Dr virus carrying a mutation in P78/83 ($Ile^{358} \rightarrow Ala^{358}$ [I358A] [8]) that compromises its ability to activate the Arp2/3 complex *in vitro* and impairs actin-based motility. The AcMNPV-3Dr-I358A mutant exhibited reduced motility speed in the nucleus (5 ± 1 μm/min) (Figure 1C), similar to what was previously observed in the cytoplasm (8 ± 3 μm/min) [6]. These results indicate that intranuclear actin-based motility depends on P78/83 and the Arp2/3 complex and suggest that viral motility contributes to the pool of dynamic nuclear F-actin observed previously [8].

Given that AcMNPV nucleocapsids use actin polymerization for movement within the nucleus and that F-actin is required for BV progeny production [9, 10], we hypothesized that nuclear actin might also play a role in egress of newly replicated viral nucleocapsids from the nucleus to the cytoplasm. It had previously been proposed that egress from the nucleus involved the association of nucleocapsids with protrusions of the nuclear envelope that project outward into the cytoplasm, the separation of these protrusions into double-membraned vesicular structures containing the virus [12], and then virus escape into the cytoplasm. However, the contribution of actin towards nuclear envelope protrusion formation and the mechanism of virus egress were unknown. Using transmission electron microscopy (TEM) to image *Spodoptera frugiperda* Sf9 and *Trichoplusia ni* High Five cells infected with AcMNPV-3mC [6] at 24 hpi, we confirmed that AcMNPV nucleocapsids were

present in double-membrane protrusions of the nuclear envelope (NE) that extended out > 0.2 μm from adjacent regions of the nuclear periphery (Figure 2A, E and F) (virus-containing double membrane structures also appear adjacent to the nucleus in individual TEM sections and may be continuous with the NE). To determine the importance of actin polymerization and depolymerization in protrusion formation, we infected cells with AcMNPV-3mC and then treated with drugs that prevent G-actin assembly (latrunculin A) or stabilize F-actin (jasplakinolide). In drug-treated cells we did not observe full NE protrusions, but instead observed small bumps in the NE that did not contain nucleocapsids and extended only ~ 0.1 μm from adjacent regions of the nuclear periphery (Figure 2C–F). We call these “nubs” to distinguish them from protrusions. Nubs could also be seen in cells with newly synthesized viral DNA that did not yet show nucleocapsid formation (data not shown). This suggests that there are two steps in virus-induced NE protrusion formation: actin-independent formation of NE nubs that precedes nucleocapsid assembly, and actin-dependent extension of longer NE protrusions. Additionally, in drug-treated cells we were unable to detect nucleocapsids in the cytoplasm by electron microscopy (Figure 2C–E), or by immunofluorescence microscopy (Figure S1B, C). These results indicate that the dynamic cycle of actin assembly and disassembly is crucial for viral movement to the nuclear periphery, extension of NE protrusions, and subsequent egress from the nucleus. Our results are also consistent with the failure of drug-treated cells to produce BV progeny [9, 10].

We also used TEM to image Sf9 and High Five cells infected with the AcMNPV-3mC-I358A mutant at 24 hpi, and we observed intermediate and cell-type specific phenotypes. The AcMNPV-3mC-I358A virus formed nubs in Sf9 cells and protrusions in High Five cells (Figure 2B, E, F). This intermediate phenotype confirms a role for intranuclear actin-based motility in the formation of NE protrusions, and is also consistent with the fact that the mutant virus can still egress from the nucleus and produce BV progeny with reduced efficiency [6].

To further investigate the role of viral actin-based motility in egress from the nucleus, we imaged moving AcMNPV-3Dr viruses at the inner nuclear periphery in live cells, first using lamin B tagged with mCherry (mCh-lamin B2) to visualize the NE (Figure 3A; Video S1, segment 2). We observed individual nucleocapsids moving within NE protrusions that resembled those seen by electron microscopy. In subsequent experiments using AcMNPV-3Dr and visualizing F-actin (using Lifeact-mCherry), we observed viruses moving in circular paths, apparently trapped within NE protrusions, with their associated actin tails forming donut-shaped rings at the nuclear periphery (Figure 3B; Video S1, segment 3). Unexpectedly, when we visualized mCherry-lamin B2 and F-actin using Lifeact tagged with TagBFP (Lifeact-TagBFP), we observed localized dissolution of fluorescent lamin B signal accompanied by a transient burst of actin polymerization (Figure 3C; Video S2, segment 1, left panel). In cases when events stayed in the focal plane of imaging, nascent actin comet tails could be visualized during egress (Video S2, segment 1, right panel) as nucleocapsids entered the cytoplasm and moved freely, unobstructed by the NE. Disruption of NE protrusions was also observed using a different NE marker, the integral inner nuclear membrane protein SUN2 tagged with triple-mCherry (SUN2-triple-mCherry) (Video S2, segment 2). These results suggest that AcMNPV egress involves actin-based movement

within NE protrusions, which is coupled with localized NE disruption, and subsequent actin-based motility in the cytoplasm.

We next sought to further test the notion that viral egress involves a local disruption of the NE, as suggested by the dissolution of fluorescent lamin B and SUN2 signals as egress occurred. To measure NE integrity, we expressed GFP tagged with a nuclear localization sequence (NLS-GFP), and then quantified the nuclear/cytoplasmic fluorescence intensity ratio of NLS-GFP per unit area (Figure 4). We found that this ratio decreased more rapidly in infected cells compared with uninfected cells during the late stage of infection (Figure 4A–C), coincident with the burst phase of nuclear actin-based motility, nuclear egress, and the appearance of moving nucleocapsids in the cytoplasm (Video S3, top panel shows infected and bottom panel shows uninfected cells. Note there was an overall decrease in NLS-GFP signal in uninfected cells due to photobleaching from long-term confocal imaging). The leaking of NLS-GFP into the cytoplasm was dependent upon actin polymerization, as addition of latrunculin A or jasplakinolide, or infecting with AcMNPV-3mC-I358A, resulted in a slower rate of decrease of the nuclear/cytoplasmic NLS-GFP that was similar to the rate in uninfected cells (Figure 4D–G). These results suggest that AcMNPV egress from the nucleus disrupts NE integrity and that this disruption requires actin polymerization/depolymerization and actin-based motility.

We also tested the alternative hypothesis that egress occurs by outward transit through the nuclear pore, as with ingress into the nucleus [6, 13]. To test the potential involvement of nuclear pores, at a time approaching the late stage of infection (prior to the burst phase of actin-based motility) we microinjected cells with fluorescently labeled wheat germ agglutinin (WGA), which blocks trafficking through nuclear pores [14] and inhibits AcMNPV ingress into the nucleus [6]. WGA did not prevent egress from the nucleus, as virions were able to escape into the cytoplasm and undergo actin-based motility following WGA injection (Figure S2A; Video S4, segment 1, WGA in left panel and EGFP-actin in right panel). Furthermore, viral egress and subsequent actin-based motility in the cytoplasm were not prevented by treating cells approaching the late stage of infection with a drug that blocks the CRM1 nuclear export pathway, leptomycin B (Video S4, segment 2). Thus, AcMNPV does not egress from the nucleus by transit through the nuclear pore complex or by using a CRM1-mediated nuclear export pathway. Together with the above-mentioned NLS-GFP studies, these results suggest that viral egress from the nucleus instead involves NE disruption and viral release into the cytoplasm.

Following egress from the nucleus, the mechanism by which AcMNPV nucleocapsids move to the plasma membrane, and the involvement of actin and/or microtubules, had remained unclear. In particular, previous studies yielded conflicting results regarding the role of microtubules, with some finding that microtubule disassembly by drug treatment and silencing of kinesin light chain by RNAi inhibited BV production [15, 16, 17], and others finding that microtubule disassembly had no effect on BV release [18]. To resolve this controversy, we reassessed the effect of two drugs that have been used to disrupt microtubules, colchicine and nocodazole, on microtubule organization and BV production. We confirmed that colchicine is effective at depolymerizing microtubules in High Five cells, whereas nocodazole is not (Figure S2B) [18, 19]. However, despite its efficacy at disrupting

microtubules, colchicine had no effect on BV release (Figure S2C). Thus, microtubules are not important for BV production. Instead, as mentioned above, we observed nucleocapsids moving by actin-based motility following egress from the nucleus, starting at 13 ± 3 hpi (Figure 1A and S3; Video S5). The speed of motility in the cytoplasm was 10 ± 3 μm/min for AcMNPV-3Dr and 5 ± 1 μm/min for the AcMNPV-3Dr-I358A mutant (Figure 1C), similar to the speeds seen during ingress [6]. Furthermore, based on the effect of actin-disrupting drugs, actin is known to be crucial for BV production [9, 10]. These results suggest that, rather than using microtubules, AcMNPV uses actin-based motility for movement to the plasma membrane, where viruses acquire an envelope to form BV progeny.

Our study indicates that AcMNPV is a prolific manipulator of actin, having evolved to harness actin-based motility to facilitate several stages of infection, including ingress of input virus to the nucleus [6], as well as egress of progeny virus from the nucleus, and movement of progeny to the plasma membrane for BV budding. Other viruses also induce NE breakdown to enable egress [1]. The mechanism employed by AcMNPV, however, which involves nuclear F-actin-dependent NE protrusion formation and disruption, has not been previously described. It may nevertheless represent a generalizable strategy for NE disruption during infection. Actin-mediated NE disruption by AcMNPV may involve rupture of inner and outer NE membranes. Alternatively, it may involve fusion of inner and outer NE membranes, which could be mediated by N-ethylmaleimide sensitive factor (NSF) or soluble NSF attachment receptor (SNARE) proteins, which are involved in AcMNPV nuclear egress [20]. Our data also points to a nucleocapsid and actin-independent process that forms NE nubs prior to nucleocapsid and actin-dependent protrusion formation. It was recently reported that a group of AcMNPV proteins interacts with components of the ESCRT-III complex and that ESCRT-III is required for nuclear egress [21], suggesting these proteins may be involved in nub formation. Interestingly, F-actin within the nucleus of uninfected cells is reported to play a role in nuclear assembly and shape [22], as well as intranuclear organization [23], particularly in large oocyte nuclei. Moreover, linkages between the outer NE and the cytoplasmic actin network have been shown to promote both NE rupture in cells with defects in nuclear lamina organization [24], and NE stabilization in cells undergoing confined migration [25]. Pathogens often evolve to activate and exaggerate existing cellular pathways, rather than inventing new pathways of their own. Therefore, studying how AcMNPV mobilizes actin for nuclear egress may reveal new cytoskeletal functions important for NE integrity, stability, and remodeling.

STAR METHODS

KEY RESOURCES TABLE

REAGENT or RESOURCE	SOURCE	IDENTIFIER
Antibodies		
mouse anti-tubulin (clone E7)	Developmental Studies Hybridoma Bank, University of Iowa	RRID: AB_2315513
goat anti-mouse FITC	Zymed	Cat# A16079; RRID:AB_2534753

REAGENT or RESOURCE	SOURCE	IDENTIFIER
mouse anti-GP64 B12D5	Loy E. Volkman	N/A
goat anti-mouse HRP	Bio-Rad labs	Cat# 170-6516; RRID:AB_11125547
Bacterial and Virus Strains		
AcMNPV WOBpos	[8]	N/A
AcMNPV-3mC	[6]	N/A
AcMNPV-3mC-I358A	[6]	N/A
BW25113/pKD46	[26]	N/A
AcMNPV-3Dr	This paper	N/A
AcMNPV-3Dr-I358A	This paper	N/A
AcMNPV-1mC	This paper	N/A
AcMNPV-3mCq	This paper	N/A
Chemicals, Peptides, and Recombinant Proteins		
colchicine	Sigma	Cat# C-9754
nocodazole	EMD Bioscience	Cat# 487928
cytochalasin D	EMD Bioscience	Cat# 250255
jasplakinolide	Calbiochem	Cat# 420127
latrunculin A	Biomol	Cat# T-119
phalloidin	Sigma	Cat# P2141
phalloidin Alexafluor-568	Invitrogen	Cat# A12380
TransIT-2020	Mirus Bio	Cat# MIR5404
TransIT-Insect	Mirus Bio	Cat# MIR6100
TrueBlue peroxidase substrate	SeraCare	Cat# 5510-0030
WGA-TRITC	Invitrogen	Cat# W7024
Experimental Models: Cell Lines		
Sf9 cells	UC Berkeley cell culture facility	
High Five cells	Dr. Shizuo G. Kamita	
TN368 cells	Dr. Loy E. Volkman	
Recombinant DNA		
plasmid: pACT-GFP-actin	[8]	N/A
plasmid: pWOBCAT	[6]	N/A
plasmid: AcMNPV-1mC	This paper	N/A
plasmid: 3mC	[6]	N/A
plasmid: AcMNPV-3mCq	This paper	N/A
plasmid: pKW2416	Dr. Karsten Weis	N/A
plasmid: pBluescript+ II	Agilent	Cat# 212207
plasmid: 3Dr	This paper	N/A
plasmid: Lifeact-mCherry	This paper	N/A
plasmid: pEGFP-N1	Clontech	Cat# 6085-1
plasmid: Lifeact-tagBFP	This paper	N/A

REAGENT or RESOURCE	SOURCE	IDENTIFIER
plasmid: pTag-BFP-N	Evrogen	Cat# FP172
plasmid: pACT-Lifeact-TagBFP	This paper	N/A
plasmid: mCherry-C2 LB2	Dr. Rebecca Heald	N/A
plasmid: pACT-mCherry-lamin B2	This paper	N/A
plasmid: pACT-NLS-GFP-actin	[31]	N/A
plasmid: pACT-NLS-GFP	This paper	N/A
plasmid: SUN2-GFP/pcDNA4	Dr. Kyle J. Roux [33]	N/A
plasmid: SUN2-3xmC	This paper	N/A
Software and Algorithms		
SPSS Statistics 25	IBM	https://www.ibm.com/analytics/us/en/technology/spss/
ImageJ	NIH Image	https://imagej.nih.gov/
GraphPad Prism 5	GraphPad Software	https://www.graphpad.com/
Metamorph 7.8	Molecular Devices	https://www.moleculardevices.com/

CONTACT FOR REAGENT AND RESOURCE SHARING

Further information and requests for reagents may be directed to and will be fulfilled by the Lead Contact, Matthew D. Welch (welch@berkeley.edu).

EXPERIMENTAL MODEL AND SUBJECT DETAILS

Cell Lines—Sf9 cells (ovarian cells from female *Spodoptera frugiperda*) were maintained in Grace's insect media (Gemini Bio-Products) with 10% fetal bovine serum (FBS; Gemini Bio-Products) or in ESF 921 media (Expression Systems) at 28°C, either in suspension or adherent culture. High Five and TN368 cells (ovarian cells from female *Trichoplusia ni*) were maintained in TNM-FH insect media (Gemini Bio-Products) with 10% FBS at 28°C in adherent culture.

Viruses—The virus used in this study was AcMNPV WOBpos, which can be propagated as a bacmid in *E. coli* [8]. The generation of AcMNPV-3mC (a virus with its *vp39* gene fusion to three copies of the gene encoding mCherry) and AcMNPV-3mC-I358A (a virus with a mutation in *p78/83* that results in the substitution of isoleucine 358 to alanine) were previously described [6]. To generate all other viruses, transfer plasmid vectors generated as described below were linearized, gel-purified, and co-electroporated with WOBpos (at least 30 fmol of linearized transfer vector with 0.2 μg of bacmid DNA) into BW25113/pKD46 *E. coli*, to introduce alterations by homologous recombination, as described previously [8]. These viruses include: AcMNPV-3Dr, a virus with an extra copy of the *vp39* gene fused to three copies of the gene encoding Dronpa [27]; AcMNPV-3Dr-I358A, a virus with an extra copy of the *vp39* gene fused to three copies of the gene encoding Dronpa as well as the I358A mutation in the *p78/*83 gene; AcMNPV-1mC, a virus with a *vp39* gene fusion to one copy of the gene encoding mCherry under the control of the viral p10 promoter; and AcMNPV-3mCq, a virus with a *vp39* gene fusion to three copies of the gene encoding mCherry that also contains two conservative nucleotide substitutions within the *vp39* gene to

eliminate the start site for transcription of the overlapping delayed early *cg30* gene and hence has reduced early mCherry expression.

METHOD DETAILS

Cloning of Viral Transfer and Expression Plasmids—The generation of a pACT plasmid that expresses EGFP-actin (pACT-GFP-actin; for insect cell expression) was previously described [28]. The transfer vector for generating AcMNPV-1mC was constructed by subcloning a fusion of the *vp39* and *mCherry* genes into the p10 WOBCAT transfer vector (containing the AcMNPV *p10* promoter (118911-118681 in the AcMNPV E2 genome; accession KM667940.1) in transfer vector pWOBCAT [6]). The transfer vector for generating AcMNPV-3mCq was constructed by introducing two conservative nucleotide substitutions (TA to CC; at positions 75907-75908 in the AcMNPV E2 genome) into transfer vector 3mC [6] that altered the start site for transcription of the delayed early *cg30* gene without altering the VP39 protein sequence. To generate the *vp39* gene fusion to three copies of the *Dronpa* gene, three separate copies of *Dronpa* were PCR amplified from pKW2416 (a kind gift from K. Weis, ETH Zurich), and the three copies (with XbaI/EcoRI, EcoRI/XhoI, and XhoI/ApaI ends) were cloned in tandem into pBSKS+ (Agilent). The three tandem copies were then fused to *vp39* with the same two mutations as in the 3mCq transfer vector, to generate 3Dr. 3Dr was moved into transfer vector pWOBGent6 [6] using BsiWI and ApaI to provide flanking regions of homologous sequences for recombination with the viral genome of WOBpos (generating AcMNPV-3Dr) and I358A (generating AcMNPV-3Dr-I358A), as described above.

The plasmid that expresses Lifeact [29] fused with mCherry (Lifeact-mCherry) was generated by PCR-amplifying the *mCherry* gene (as described in reference [6], but with XbaI and EcoRI sites), subcloning into the plasmid pEGFP-N1 (Clontech) containing the *Lifeact* gene [30], and then transferring *Lifeact-mCherry* (with SpeI and BglII ends) into pACT [31]. The plasmid that expresses Lifeact tagged with three tandem copies of TagBFP [32] (Lifeact-TagBFP) was constructed by subcloning two (AvaI/blunt and blunt/BamHI cut) copies of TagBFP from pTagBFP-N (Evrogen) into Lifeact GFP vector [30]. A third copy of TagBFP (blunt/NotI) was then inserted into blunt/NotI cut plasmid, and this gene encoding Lifeact with three copies of TagBFP (blunt/NotI) was transferred into pACT (SmaI/NotI cut) for expression in insect cells (pACT-Lifeact-TagBFP). The plasmid expressing mCherry-Lamin B2 (human lamin B2) was constructed by cutting the corresponding gene from plasmid mCherry-C2 LB2 (a kind gift from R. Heald) and inserting the blunt/XbaI fragment into SmaI/XbaI cut pACT (to generate pACT-mCherry-lamin B2). The plasmid expressing NLS-GFP was constructed by cutting the gene encoding NLS-GFP from NLS-GFP-actin/pACT [31] and inserting the blunt/BamHI fragment into blunt/BamHI cut pACT (to generate pACT-NLS-GFP). The plasmid expressing SUN2 fused to three copies of the *mCherry* gene (SUN2-3xmC) was constructed by PCR amplifying SUN2 from SUN2-GFP/pcDNA4 [33] (a kind gift from K. Roux), cloning it into p10-3mC (same as 3mC described above, but with a baculovirus very late *p10* promoter driving *vp39-triple mCherry*), and then moving SUN2-triple-mCherry into pACT by inserting a blunt-SalI fragment into pACT (blunt/XhoI cut).

Immunofluorescence and Live Cell Imaging—To visualize microtubules in High Five cells, 7.5×10^4 cells were plated to 22 mm^2 coverslips and allowed to settle for 1 h, after which fresh media containing either colchicine (10 μM) or nocodazole (80 μM) was added. After 4 h, coverslips were fixed with 4% formaldehyde in PHEM (60 mM PIPES, 25 mM HEPES, 10 mM EGTA, 2 mM $MgCl_2$, pH 6.9) for 10 min, rinsed in PHEM, and then fixed in methanol for 3 min at −20°C. Following rinsing, coverslips were treated with E7 anti-tubulin antibody (Developmental Studies Hybridoma Bank, University of Iowa) and subsequently a goat anti-mouse secondary antibody linked to FITC (Zymed). In experiments to detect nucleocapsids in the cytoplasm, 2.25×10^5 High Five cells were plated to coverslips and settled overnight, followed by inoculation with AcMNPV-3Dr at a multiplicity of infection (MOI) of ~30. At 12 hpi, media containing cytochalasin D (EMD Bioscience; 1 μg/ml), jasplakinolide (Calbiochem; 1 μM) or latrunculin A (Biomol; 4 μM) was added. Coverslips were pre-extracted at 18 hpi in 0.1% Triton-X-100/cytoskeleton buffer (10 mM MES pH 6.1, 138 mM KCl, 3 mM $MgCl_2$, 2 mM EGTA) containing 0.32 M sucrose, and 1 μg/ml phalloidin [6], fixed in 4% formaldehyde in PHEM, then actin was stained with phalloidin Alexafluor-568 (Invitrogen) and DNA with DAPI (Invitrogen). Cells were selected for analysis based on the presence of virogenic stroma (detected by the presence of bright DAPI nuclear foci as well as nuclear capsid signal), signifying late stage viral infection.

For time-lapse imaging to visualize AcMNPV-induced nuclear and cytoplasmic actin comet tails, High Five cells were plated to 35 mm coverslip dishes (MatTek) at 2.4×10^5 to 4.0×10^5 cells per dish, in 2 ml of media, and infected with AcMNPV-3Dr or AcMNPV-3Dr-I358A at an MOI of ~10, with images captured at 5 s intervals between 9 and 20 hpi. Cells were selected for time-lapse imaging based on the presence of actin comet tails in the nucleus or cytoplasm. For visualization of actin comet tails within protrusions of the nuclear membrane and in the cytoplasm, AcMNPV-3Dr virus was used at an MOI of ~50. For NLS-GFP experiments, AcMNPV-3mCq virus was used at an MOI of ~40, and images were captured at 15 min intervals. Cells were selected for time-lapse imaging based on an initial high contrast ratio of nuclear to cytoplasmic GFP signal, as well as virus-expressed VP39-mCherry (present at a very low level at the start of imaging).

Transient transfections into cells were performed using the TransIT-2020 or TransIT-Insect reagents (Mirus Biologicals) according to the manufacturer's protocol. In all experiments, cells were transfected 1 d post-plating with plasmids expressing fluorescent protein fusions (the amount of DNA transfected into cells was 0.05–0.2 μg for pACT-Lifeact-mCherry, 1 μg pACT-mCherry-Lamin B2, 20 μg pACT-Lifeact-TagBFP, 0.04 μg pACT-NLS-GFP, 5 μg pACT-GFP-actin). Images of virus-induced actin structures were captured at 5 s intervals with the exception of nuclear envelope rupture videos, for which images were captured at 10 s intervals. For NLS-GFP experiments, high five cells were transfected with pACT-NLS-GFP two days in advance of imaging, which commenced at ~9 hpi.

Microscopy was performed using a Nikon Ti Eclipse confocal microscope with a Yokogawa CSU-XI spinning disc, 100X (1.4 NA) Plan Apo objective, a Clara Interline CCD camera (Andor Technology), and MetaMorph software (Molecular Devices). Images were processed using ImageJ software [34].

Blockage of Nuclear Pores and CRM1/Exportin 1 Export—To observe whether nuclear pore blockage hinders virus escape from the nucleus, cells were microinjected with wheat germ agglutinin (WGA). High Five cells knocked from four confluent 25 cm^2 T-flasks (transfected with 7 μg of GFP-actin/pACT plasmid) were settled to coverslip dishes by sequentially plating 5.4×10^6 cells (after 2 min cells are removed and fresh cells are plated, repeated for a total of 4 plating steps; healthy cells adhere rapidly while unhealthy cells take longer to adhere). Dishes were inoculated with 600 μl of pre-warmed WOBpos (~2×10^7 PFU). At 16 hpi, cells were microinjected with WGA-TRITC (0.5 mg/ml), using Femtotips with a FemtoJet microinjector controlled with an InjectMan micromanipulator (all from Eppendorf), using a pressure of 80 hPa, a time of 0.4 s, and a compensation pressure of 30 hPa [6]. Cells were visualized on a spinning disc confocal microscope at 28°C from ~18 hpi. Unhindered viral escape from the nucleus was assessed by the appearance of actin comet tails in the cytoplasm after microinjected cells showed WGA signal at the nuclear periphery.

To test if AcMNPV uses the CRM1/exportin 1 export pathway to escape the nucleus, 3.6×10^5 High Five cells were settled in 2 ml of media to 35 mm coverslip dishes (MatTek) overnight, then transfected with 5 μg of pACT-GFP-actin. One day post-transfection, cells were infected with AcMNPV-3mC virus at an MOI of ~50. At 14 hpi, cells with nuclear mCherry-VP39 signal were identified, media containing leptomycin B (to a final concentration of 25 ng/ml) was added, and cells were imaged at 10 min intervals overnight, as described above for WGA.

Electron Microscopy—For transmission electron microscopy, 2.5×10^6 Sf9, 2.5×10^6 TN368, or 1.3×10^6 High Five cells were plated to 6 cm dishes and inoculated with AcMNPV-3mC or AcMNPV-3mC-I358A virus at an MOI of 10. At 20 hpi, cells were washed with 100 mM sodium cacodylate (pH 7.2) with 2% sucrose, fixed in 2% glutaraldehyde, 100 mM cacodylate, and 2% sucrose for 5 min, scraped from the plastic substrate, and further fixed overnight in fresh fixative plus 0.3% BSA. Cells were then washed with 0.1 M sodium cacodylate (pH 7.2) and post-fixed in 1% osmium tetroxide, 0.8% potassium ferricyanide 1 h, washed in 0.1 M sodium cacodylate, then water, and stained in 1% uranyl acetate in 50 mM sodium maleate pH 5.2 for 1 h. Samples were washed with water and dehydrated in increasing concentrations of acetone before being infiltrated with resin for sectioning. Once on grids, sections were stained with 2% uranyl acetate in 70% methanol, rinsed in decreasing concentrations of methanol, and stained with Reynolds lead citrate. Images were captured using a Tecnai 12 (120 KV) transmission electron microscope.

Viral Growth Curves—To assess viral growth, 4.4×10^6 Sf9 cells were plated to 6 cm dishes and infected with WOBpos or AcMNPV-3Dr at an MOI of 10. After a 1 h adsorption period, cells were rinsed three times with fresh media, and then media was added containing 10 μM colchicine or 80 μM nocodazole or no drug. Growth curves were performed by taking aliquots at specified times which and freezing them at −80°C until titration was performed by plaque assay. For plaque enumeration, 6.8×10^4 Sf9 cells were plated onto 5 mm diameter wells (on 12 well slides), inoculated with 10 μl of virus dilution (4 wells/dilultion) for 1 h, then following removal of the inoculum, overlaid with ~40 μl of 0.6% methylcellulose in

Grace's media with 10% FBS [6]. After 3 d, assays were processed by fixation with 45% acetone and 25% formalin in phosphate buffer (5 mM Na_2HPO_4, 24 mM KH_2PO_4) and stained with a primary mouse antibody against the viral glycoprotein GP64, then a goat anti-mouse secondary antibody linked to HRP. TrueBlue peroxidase substrate (KPL) was then added and after mounting coverslips on slides, plaques were identified and quantified as patches of blue-staining cells.

QUANTIFICATION AND STATISTICAL ANALYSIS

Statistical Analyses—Statistical details (statistical test used, number of samples, and p values) for each experiment can be found in the Figure labels or legends. Statistical analyses of average times of virus-induced events, nucleocapsid speeds, NE protrusion heights, average GFP intensity density ratios, linear regressions, and viral growth curves were conducted using Prism (Graph Pad Software). Statistical significance was determined by one-way ANOVA analysis with Tukey's post tests for multiple comparisons. Asterisks indicate the corresponding statistical significance: **p<0.01, ***p<0.001, and n.s.=non-significant. For analysis of the slopes of the linear regressions of average GFP intensity density ratios, SPSS Statistics (IBM) was used. Based on a linear mixed model analysis, the rate of decrease of the fluorescence intensity signal per unit area of the uninfected, AcMNPV-3mC-I358A virus infection, jasplakinolide, and latrunculin A treatments were significantly different from the AcMNPV-3mC treatment ($p < 0.001$).

Supplementary Material

Refer to Web version on PubMed Central for supplementary material.

Acknowledgments

The authors wish to acknowledge the following people for contributions and support for the work in this manuscript: Loy E. Volkman for her advice, expertise, and role as a pioneer in the field of baculovirus host-pathogen interactions; Karsten Weis for sharing his knowledge of nuclear transport and aiding in experimental design; Kent McDonald and Reena Zalpuri of the UC Berkeley Electron Microscope Lab and Paul Webster for their expertise, advice, and technical aid with electron microscopy; Holly L. Aaron and Jen-Yi Lee of the UC Berkeley Molecular Imaging Center for their expertise and support for our microscopy work; Elizabeth Purdom, Boying Gong, and Hao Lyu of the UC Berkeley Department of Statistics; Rob Kern of Eppendorf Inc. for consultation on microinjection; and Rebecca Heald, Elisa Dultz, Leslie H. Stanton, Daniel L. Levy, Anne-Lore Schlaitz, and Kyle J. Roux for providing plasmid constructs and advice. This work was supported by grants R01 GM059609 and R35 GM127108 from the NIH/NIGMS (M.D.W.).

References

1. Mettenleiter TC. Breaching the barrier- the nuclear envelope in virus infection. J Mol Biol. 2016; 428:1949–1961. [PubMed: 26522933]
2. Van Oers MM, Pijlman GP, Vlak JM. Thirty years of baculovirus-insect cell protein expression: from dark horse to mainstream technology. J Gen Virol. 2014; 96:6–23. [PubMed: 25246703]
3. Szewczyk B, Hoyos-Carvajal L, Paluszek M, Skrzecz I, Lobo de Souza M. Baculoviruses-re-emerging biopesticides. Biotechnol Adv. 2006; 24:143–160. [PubMed: 16257169]
4. Makkonen KE, Airenne K, Yla-Herttulala S. Baculovirus-mediated gene delivery and RNAi applications. Viruses. 2015; 7:2099–2125. [PubMed: 25912715]
5. Welch MD, Way M. Arp2/3-mediated actin-based motility: a tail of pathogen abuse. Cell Host Microbe. 2013; 14:242–255. [PubMed: 24034611]

6. Ohkawa T, Volkman LE, Welch MD. Actin-based motility drives baculovirus transit to the nucleus and cell surface. J Cell Biol. 2010; 190:187–195. [PubMed: 20660627]
7. Mueller J, Pfanzelter J, Winkler C, Narita A, LeClainche C, Nemethova M, Carlier MF, Maeda Y, Welch MD, Ohkawa T, et al. Electron tomography and simulation of baculovirus actin comet tails support a tethered filament model of pathogen propulsion. PLoS Biol. 2014; 12:e1001765. [PubMed: 24453943]
8. Goley ED, Ohkawa T, Mancuso J, Woodruff JB, D'Alessio JA, Cande WZ, Volkman LE, Welch MD. Dynamic nuclear actin assembly by Arp2/3 complex and a baculovirus WASP-like protein. Science. 2006; 314:464–467. [PubMed: 17053146]
9. Volkman LE. *Autographa californica* MNPV nucleocapsid assembly: inhibition by cytochalasin D. Virology. 1988; 163:547–553. [PubMed: 3281373]
10. Ohkawa T, Volkman LE. Nuclear F-actin is required for AcMNPV nucleocapsid morphogenesis. Virology. 1999; 264:1–4. [PubMed: 10544124]
11. Virtanen JA, Vartiainen MK. Diverse functions for different forms of nuclear actin. Curr Opin Cell Biol. 2017; 46:33–38. [PubMed: 28092729]
12. Granados RR, Lawler KA. *In vivo* pathway of *Autographa californica* baculovirus invasion and infection. Virology. 1981; 108:297–308. [PubMed: 18635031]
13. Au S, Wu W, Zhou L, Theilmann DA, Pante N. A new mechanism for nuclear import by actin-based propulsion used by a baculovirus nucleocapsid. J Cell Sci. 2016; 129:2905–2911. [PubMed: 27284005]
14. Finlay DR, Newmeyer DD, Price TM, Forbes DJ. Inhibition of *in vitro* nuclear transport by a lectin that binds to nuclear pores. J Cell Biol. 1987; 104:189–200. [PubMed: 3805121]
15. Biswas S, Blissard GW, Theilmann DA. *Trichoplusia ni* kinesin-1 associates with *Autographa californica* Multiple Nucleopolyhedrovirus nucleocapsid proteins and is required for production of budded virus. J Virol. 2016; 90:3480–3495. [PubMed: 26763996]
16. Danquah JO, Botchway S, Jeshtadi A, King LA. Direct interaction of baculovirus capsid proteins VP39 and EXON0 with kinesin-1 in insect cells determined by fluorescence resonance energy transfer-fluorescence lifetime imaging microscopy. J Virol. 2012; 86:844–853. [PubMed: 22072745]
17. Fang M, Nie Y, Theilmann DA. AcMNPV EXON0 (Ac141) which is required for the efficient egress of budded virus nucleocapsids interacts with beta-tubulin. Virology. 2009; 385:496–504. [PubMed: 19155039]
18. Volkman LE, Zaal KJ. *Autographa californica* M nuclear polyhedrosis virus: microtubules and replication. Virology. 1990; 175:292–302. [PubMed: 2408230]
19. Carpentier DC, Griffiths CM, King LA. The baculovirus P10 protein of *Autographa californica* nucleopolyhedrovirus forms two distinct cytoskeletal-like structures and associates with polyhedral occlusion bodies during infection. Virology. 2007; 371:278–291. [PubMed: 17991504]
20. Guo Y, Yue Q, Gao J, Wang Z, Chen YR, Blissard GW, Liu TX, Li Z. Roles of cellular NSF protein in entry and nuclear egress of budded virions of *Autographa californica* multiple nucleopolyhedrovirus. J Virol. 2017; 91:e01111–17. [PubMed: 28747507]
21. Yue Q, Yu Q, Yang Q, Xu Y, Guo Y, Blissard GW, Li Z. Distinct Roles of Cellular ESCRT-I and ESCRT-III Proteins in Efficient Entry and Egress of Budded Virions of Autographa californica Multiple Nucleopolyhedrovirus. J Virol. 2018; 92:e01636–17. [PubMed: 29046462]
22. Krauss SW, Chen C, Penman S, Heald R. Nuclear actin and protein 4.1: essential interactions during nuclear assembly *in vitro*. Proc Natl Acad Sci U S A. 2003; 100:10752–10757. [PubMed: 12960380]
23. Feric M, Brangwynne CP. A nuclear F-actin scaffold stabilizes ribonucleoprotein droplets against gravity in large cells. Nat Cell Biol. 2013; 15:1253–1259. [PubMed: 23995731]
24. Hatch EM, Hetzer MW. Nuclear envelope rupture is induced by actin-based nucleus confinement. J Cell Biol. 2016; 215:27–36. [PubMed: 27697922]
25. Skau CT, Fischer RS, Gurel P, Thiam HR, Tubbs A, Baird MA, Davidson MW, Piel M, Alushin GM, Nussenzweig A, et al. FMN2 makes perinuclear actin to protect nuclei during confined migration and promote metastasis. Cell. 2016; 167:1571–1585. [PubMed: 27839864]

26. Datsenko KA, Wanner BL. One-step inactivation of chromosomal genes in *Escherichia coli* K-12 using PCR products. Proc Natl Acad Sci USA. 2000; 97:6640–6645. [PubMed: 10829079]
27. Ando R, Mizuno H, Miyawaki A. Regulated fast nucleocytoplasmic shuttling observed by reversible protein highlighting. Science. 2004; 306:1370–1373. [PubMed: 15550670]
28. Ohkawa T, Rowe AR, Volkman LE. Identification of six *Autographa californica* multicapsid nucleopolyhedrovirus early genes that mediate nuclear localization of G-actin. J Virol. 2002; 76:12281–12289. [PubMed: 12414968]
29. Riedl J, Crevenna AH, Kessenbrock K, Yu JH, Neukirchen D, Bista M, Bradke F, Jenne D, Holak TA, Werb Z, et al. Lifeact: a versatile marker to visualize F-actin. Nat Methods. 2008; 5:605–607. [PubMed: 18536722]
30. Serio AW, Jeng RL, Haglund CM, Reed SC, Welch MD. Defining a core set of actin cytoskeletal proteins critical or actin-based motility of rickettsia. Cell Host Microbe. 2010; 7:388–398. [PubMed: 20478540]
31. Gandhi KM, Ohkawa T, Welch MD, Volkman LE. Nuclear localization of actin requires AC102 in *Autographa californica* multiple nucleopolyhedrovirus-infected cells. J Gen Virol. 2012; 93:1795–1803. [PubMed: 22592260]
32. Subach OM, Gundorov IS, Yoshimura M, Subach FV, Zhang J, Gruenwald D, Souslova EA, Chudakov DM, Verkhusha VV. Conversion of red fluorescent protein into a bright blue probe. Chem Biol. 2008; 15:1116–1124. [PubMed: 18940671]
33. Liu Q, Pante N, Misteli T, Crisp M, Hodzic D, Burke B, Roux KJ. Functional association of Sun1 with nuclear pore complexes. J Cell Biol. 2007; 178:785–798. [PubMed: 17724119]
34. Schneider CA, Rasband WS, Eliceiri KW. NIH Image to ImageJ: 25 years of image analysis. Nat. Methods. 2012; 9:671–675. [PubMed: 22930834]

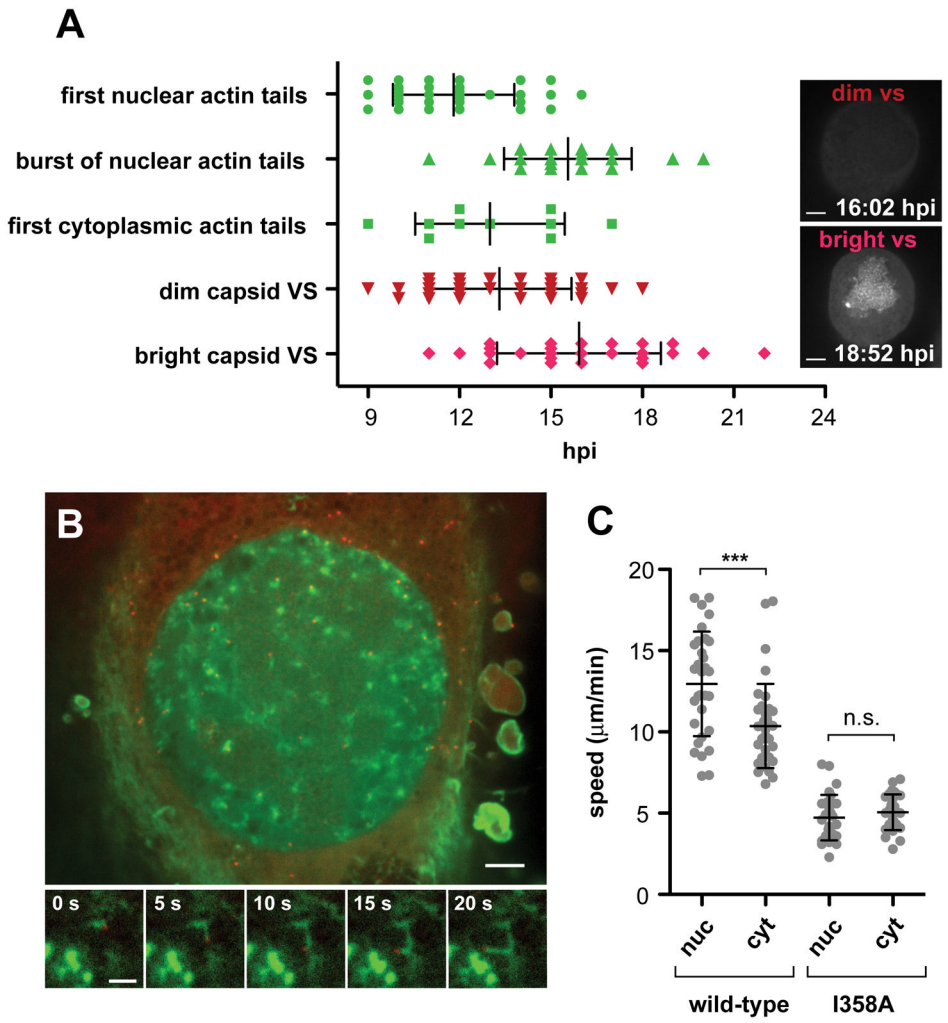

Figure 1. AcMNPV undergoes actin-based motility in the nucleus during the late stage of infection

(**A**) Timeline of post-replicative events visualized by F-actin and major capsid protein VP39 markers. High Five cells expressing Lifeact-mCherry (green; to visualize F-actin) were infected with wild-type AcMNPV-3Dr (red; to visualize VP39), and images were captured at 15-min intervals. The first detectable instances of the following key viral late stage events were tallied: actin tails in the nucleus; actin tails in the cytoplasm; the burst phase of nuclear actin tails, where many appear within a ~75 min window; the virogenic stroma (VS) as seen by VP39 signal; and a well-developed VS as viral production increases. Mean times in hpi ± SD are indicated by the vertical bars. Inset images show examples of dim VS versus bright VS in infected High Five cells. Scale bars, 5 μm. (**B**) Upper panel: actin tails (green; Lifeact-mCherry) in the nucleus of a High Five cell infected with AcMNPV-3Dr (red). Scale bar, 5 μm. Lower panels: time series of live cell imaging as in upper panel, showing actin-based motility within the nucleus, at 5 s intervals. Scale bar, 2 μm. (**C**) Speed of AcMNPV nucleocapsids moving by actin-based motility within the nucleus, and then following escape into the cytoplasm (nuc- speed within the nucleus; cyt- speed within the cytoplasm; wild-type is AcMNPV-3Dr; I358A is AcMNPV-3Dr-I358A mutant virus). Data were taken for 30

nucleocapsids of each virus. Dots represent individual nucleocapsid speed measurements. Mean speed ± SD are indicated by horizontal bars. Statistical comparisons by one-way ANOVA with Tukey's post-tests; n.s.= non-significant, ***=p<0.001. See also Figure S1 and Video S1.

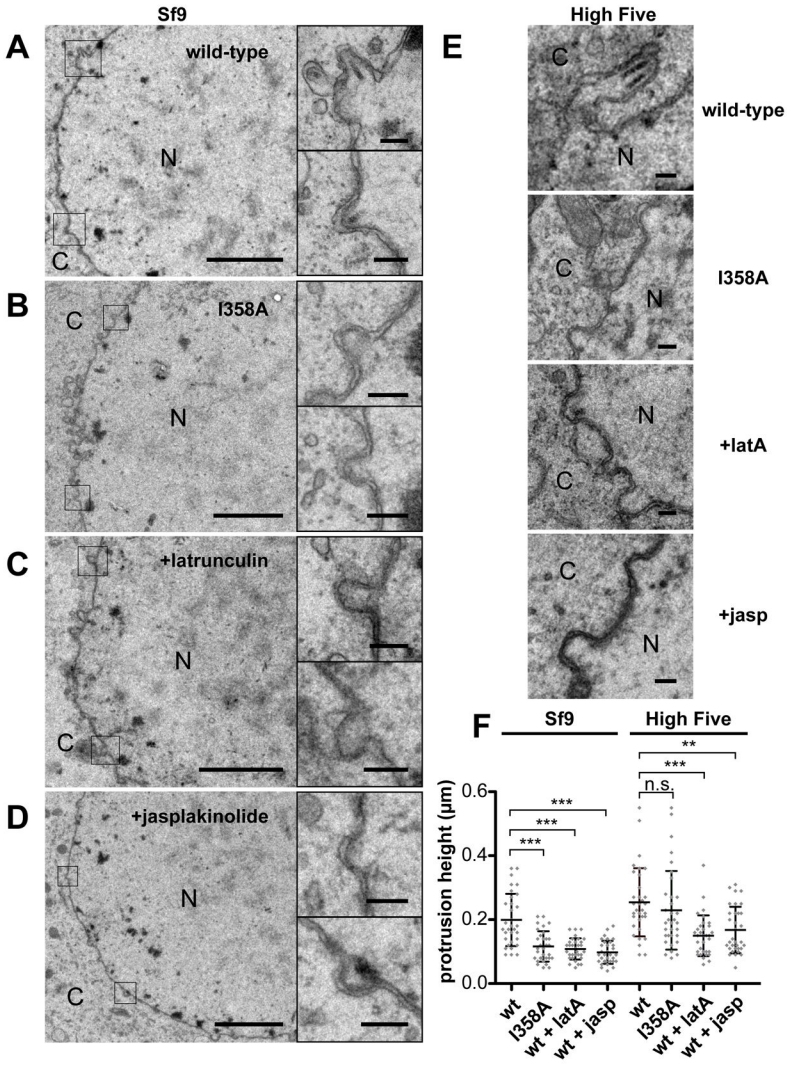

Figure 2. AcMNPV requires actin to form protrusions in the nuclear envelope during the late stage of infection

(**A**) Wild type AcMNPV-3mC infected Sf9 cell at 24 hpi. Boxed areas are magnified to the right show nuclear envelope protrusions with nucleocapsids. Left: Scale bar, 5 μm. Right: Scale bar, 0.2 μm. (**B**) AcMNPV-3mC-I358A infected Sf9 cell at 24 hpi. Boxed areas magnified to the right show nuclear envelope nubs without nucleocapsids. Left: Scale bar, 5 μm. Right: Scale bar, 0.2 μm. (**C**) Latrunculin A-treated AcMNPV-3mC infected Sf9 cell at 24 hpi. Boxed areas magnified to the right show nuclear envelope nubs without nucleocapsids. Left: Scale bar, 5 μm. Right: Scale bar, 0.2 μm. (**D**) Jasplakinolide-treated AcMNPV-3mC infected Sf9 cell at 24 hpi. Boxed areas magnified to the right show nuclear envelope nubs without nucleocapsids. Scale bar, 5 μm. Right: Scale bar, 0.2 μm. (**E**) High Five cells infected with AcMNPV-3mC (top), AcMNPV-3mC-I358A (top middle), or AcMNPV-3mC and treated with latrunculin A (bottom middle) or jasplakinolide (bottom), all at 24 hpi. Scale bar, 0.2 μm. For (A-E): N = nucleus, C = cytoplasm. (**F**) Protrusion or nub heights in Sf9 and High Five cells. Dots represent individual protrusion or nub heights. Mean height ± SD are indicated by horizontal bars. Statistical comparisons by one-way

ANOVA with Tukey's post-tests; n.s.= non-significant, **=p<0.01, ***=p<0.001. See also Figure S1.

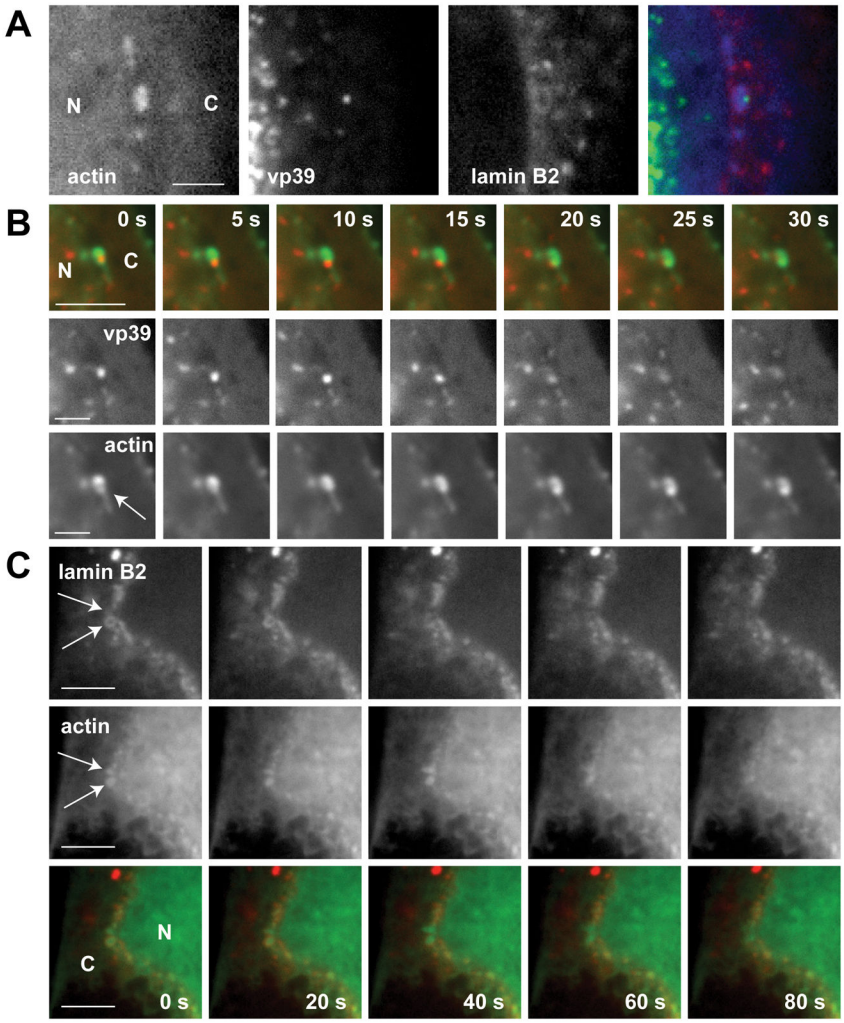

Figure 3. AcMNPV moves within and then disrupts and exits protrusions of the nuclear envelope

(**A**) Still image of wild type AcMNPV-3Dr nucleocapsid (VP39; green) and F-actin (Lifeact-TagBFP; blue) bounded by lamin B2 (mCherry-lamin B2; red) in a live High Five cell at 19.2 hpi. Scale bar, 3 μm. (**B**) Time series (at 5 s intervals) of a moving AcMNPV-3Dr nucleocapsid (VP39; red) and F-actin (Lifeact-mCherry; green) at the nuclear periphery in a High Five cell at 27.1 hpi. Arrow points to the actin tail which forms a donut-shaped ring. Scale bar, 3.3 μm. (**C**) Disruption of the nuclear envelope by AcMNPV-3Dr as seen by the loss of lamin B2 (mCherry-lamin; red), and the accompanying burst of F-actin (Lifeact-TagBFP; green), in a High Five cell at 24 hpi. Scale bar, 5 μm. Arrows point to the protrusions in the nuclear envelope. N - nucleus, C- cytoplasm. See also Figures S2, and S3; and Videos S2, S3, S4 and S5.

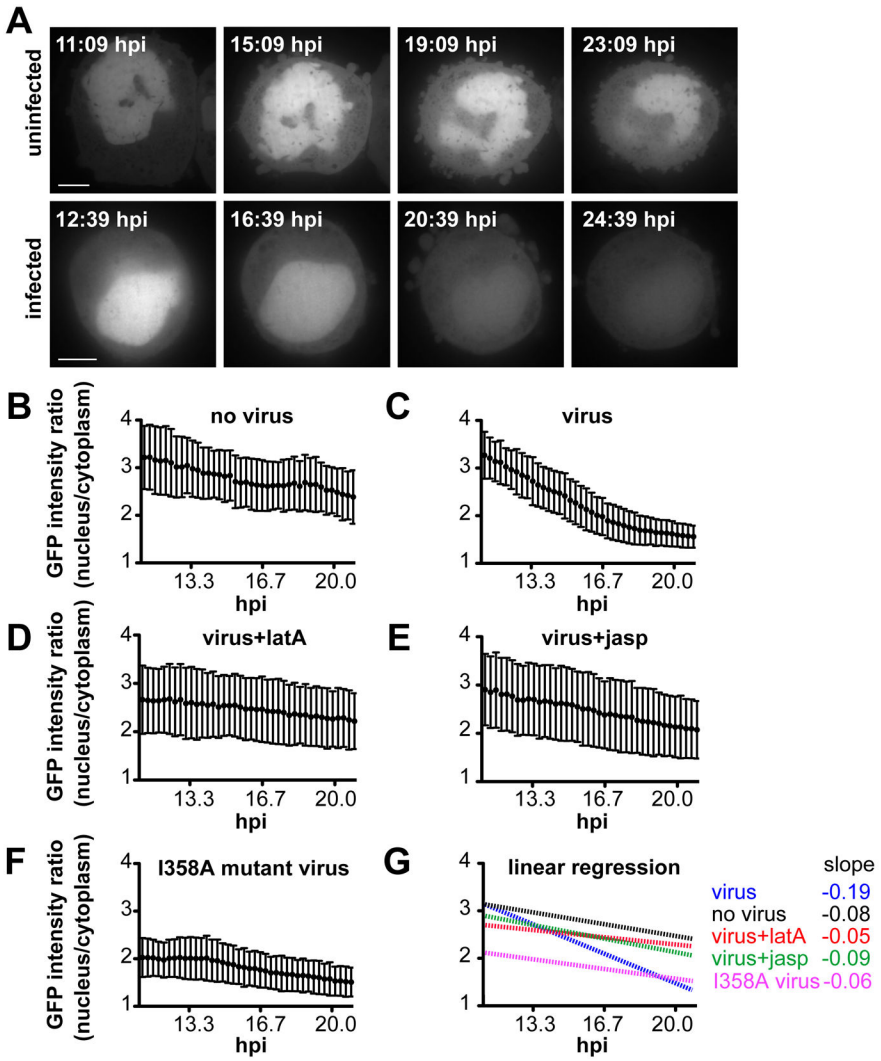

Figure 4. Nuclear envelope integrity is compromised during the late stage of AcMNPV infection by an actin-dependent mechanism

(**A**) Time series of NLS-GFP localization in uninfected (top panels) and wild type AcMNPV-3mCq infected (bottom panels) High Five cells. Time in hr:min. Scale bar, 10 μm. (**B–F**) Plots of GFP intensity ratio (nucleus/cytoplasm) per unit area over time for (B) uninfected, (C) AcMNPV-3mCq infected, (D) AcMNPV-3mCq infected with latrunculin, (E) AcMNPV-3mCq infected with jasplakinolide, or (F) AcMNPV-3mCq-I358A infected. Dots show the mean for 30 cells at each time point. Error bars are SD. (**G**) A linear regression panel shows line fits for each treatment, with slope values for each line. Based on linear mixed model analysis, the slopes of the GFP intensity ratios of were significantly different for infected but untreated cells, versus uninfected, jasplakinolide-treated, latrunculin A-treated, or I358A-infected cells ($p < 0.001$). See also Video S3.